

Biomass-Based N, P, and S Self-Doped Porous Carbon for High-Performance Supercapacitors

Guangzhen Zhao,^{†,‡} Yanjiang Li,[‡] Guang Zhu,[§] Junyou Shi,^{*,†,||} Ting Lu,^{*,‡,§,¶} and Likun Pan^{‡,¶}

[†]Energy Resources and Power Engineering College, Northeast Electric Power University, 169 Changchun Road, Jilin 132012, PR China

[‡]Shanghai Key Laboratory of Magnetic Resonance, School of Physics and Materials Science, East China Normal University, 3663 North Zhongshan Road, Shanghai 200062, PR China

[§]Anhui Key Laboratory of Spin Electron and Nanomaterials (Cultivating Base), Suzhou University, Educational Park, Suzhou 234000, PR China

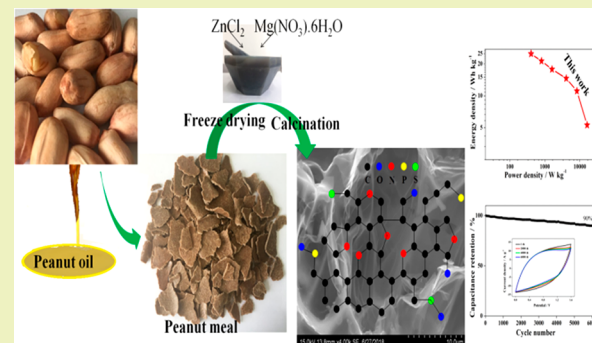
^{||}Forestry College, Beihua University, 3999 Binjiang East Road, Jilin 132013, PR China

[¶]Department of Chemical Engineering, School of Environmental and Chemical Engineering, Shanghai University, 99 Shangda Road, Shanghai 200444, PR China

Supporting Information

ABSTRACT: Biomass-based hierarchically porous carbon is green and eco-friendly, which exhibits a wide potential for energy storage due to its large specific surface area and multiheteroatoms codoping. Herein, nitrogen (N), phosphorus (P), and sulfur (S) self-doped hierarchically porous carbon (N–P–S-HPC) has been prepared by a one-step method from a peanut meal for the first time. The as-prepared N–P–S-HPC possesses a typical hierarchically porous framework (micropores, mesopores, and macropores) with an extremely large specific surface area ($2090 \text{ m}^2 \text{ g}^{-1}$) and N (11.2 atomic %), P (0.82 atomic %), and S (0.64 atomic %) doping. N–P–S-HPC as an electrode for supercapacitors displays an ultrahigh specific capacitance of 525 F g^{-1} (1 A g^{-1}) with the contributions of electrical double layer capacitance (EDLC) and pseudocapacitance (PC). Remarkably, the capacitance retention of N–P–S-HPC reaches up to 68% (10 A g^{-1}). The N–P–S-HPC//N–P–S-HPC symmetrical supercapacitor delivers a maximum energy density (24.9 Wh kg^{-1} at 400 W kg^{-1}). After 6000 cycles at 300 mV s^{-1} , the capacitance loss is only 10%, indicating excellent cycling stability of the peanut meal converted N–P–S-HPC, which enables it to be a promising candidate for energy storage and renewable delivery devices.

KEYWORDS: Peanut meal, Heteroatom self-doped, Porous carbon, Large specific surface area, Supercapacitors



INTRODUCTION

To overcome increasingly deteriorative environmental issues and alleviate the consumption of petroleum and coal resources, it is imperative to develop eco-friendly, efficient, and low-cost energy storage technologies,^{1–5} such as solar cells,⁶ photocatalytic water splitting,^{7,8} supercapacitors (SCs),⁹ lithium ion batteries,¹⁰ and so on. Especially in recent years, SCs, also called ultracapacitors, have received tremendous attention in various electronics markets, such as portable electronic components, power backups, hybrid or electrical vehicles, owing to their long cycle life, rapid charge–discharge rate, and large power density and so on, compared with other energy storage devices.^{11–15} However, the major challenge for the most commercial SCs is their inferior energy density, which impedes their applications in large energy consuming devices.

As known, the energy density for SCs is proportional to the capacitive performance of electrode materials.¹¹ Herein, it is necessary to enhance the capacitance. For the traditional

electrical double-layer capacitors (EDLCs), the charge storage mainly roots from nonfaradic charge gathered on the surface, which mainly depends on specific surface area and appropriate pore sizes of the electrode.^{16–18} Carbon electrode materials with outstanding electrochemical performances (e.g., graphene,¹⁹ carbon nanotubes,²⁰ porous carbons,²¹ carbon nanofibers,²² and so on) have attracted extensive interest. Especially, porous carbon materials, owing to the simple facility, low cost, and abundant resources, have been widely utilized as an electrode for SCs.²³ However, the electric double layer mechanism limits the capacitive performance of carbon materials.

Introducing heteroatoms (e.g., N,^{24–27} P,²⁸ S,^{29,30} and B³¹) into the carbon matrix is expected as one of the most effective

Received: February 3, 2019

Revised: June 3, 2019

Published: June 24, 2019

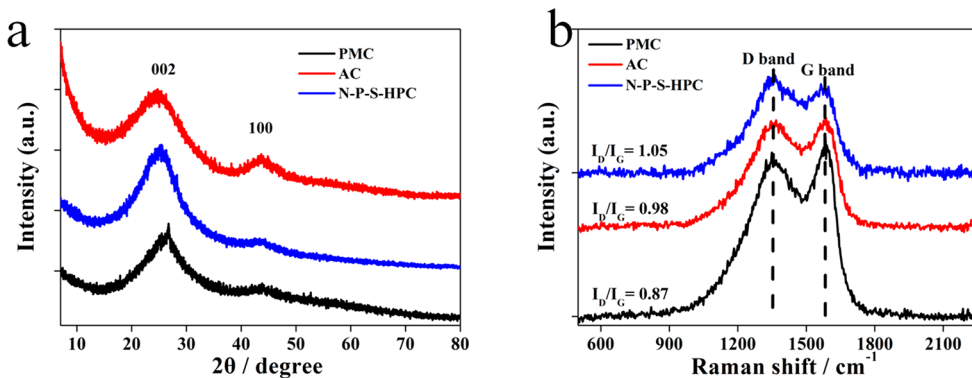


Figure 1. XRD patterns (a) and Raman spectra (b) of PMC, AC, and N–P–S–HPC.

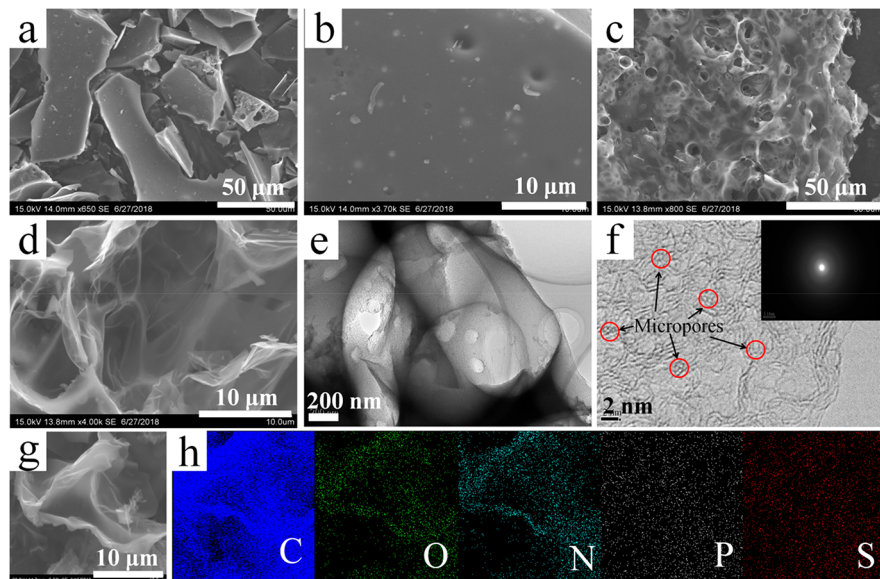


Figure 2. SEM images of PMC (a, b). SEM images of N–P–S–HPC (c, d). TEM (e) and HRTEM (f) images of N–P–S–HPC. The inset of part f is the SAED pattern. SEM image of N–P–S–HPC (g) and corresponding elemental mapping images of C, O, N, P, and S (h).

approaches to enhance the capacitive performance of SCs by combining of the electrical double-layer and pseudocapacitive characteristics.^{32,33} Furthermore, functional groups with heteroatoms can also decrease the charge transfer resistance of carbon electrodes as well as improve the wettability to the electrolyte, which benefits the electrochemical performance.^{29,34,35} Therefore, biomass converted porous carbon materials have been widely utilized as effective precursors for SCs due to the heteroatom self-doping, green resource, and low cost.^{36–38} According to previous reports, carbons derived from biomasses after activation treatment exhibit hierarchically porous framework structure with large specific surface areas.^{39,40} For instance, Long et al. reported that after KOH chemical activation, the obtained porous carbon exhibited a higher capacitive performance (374 F g^{-1} at 0.5 A g^{-1}) than primeval carbon (116 F g^{-1}).⁴¹ Activated carbon (AC) from biomass waste material with a large specific area ($1771 \text{ m}^2 \text{ g}^{-1}$) was prepared by Lu et al. and displayed a higher capacitive performance (222 F g^{-1} at 1 A g^{-1}) using KOH as an activation agent.⁴² Meanwhile, rational design and synthesis of nanostructures can also improve the electrical property of the materials.^{6,43–47} Up until now, various types of biomasses have been reported as precursors for porous carbons with outstanding capacitive performances.^{9,10} For example, wheat

flour-based hierarchically porous framework structure carbon material with N doping was reported for SCs with a high capacitive performance (383 F g^{-1} at 1 A g^{-1}).³⁶ Gelatin-based porous carbon nanosheets with B and N codoping displayed a high specific capacitance (268 F g^{-1} at 0.1 A g^{-1}).⁴⁰ Peanut meal (PM), byproduct of the extraction of peanut oil with N (7 atomic %), P (2.49 atomic %), and S (0.96 atomic %) elements, can be directly used as a precursor for N, P, and S codoped porous carbon. Unfortunately, few reports have been available for the hierarchically porous carbons originating from PM used as SCs electrodes. Herein, we employ a one-step process by simultaneous carbonization and activation to synthesize N, P, and S codoped hierarchical porous carbon (N–P–S–HPC) material from PM. The obtained N–P–S–HPC with a large specific surface area and rich N, P, and S contents exhibits outstanding electrochemical performances for SCs.

EXPERIMENTAL SECTION

Synthesis of N–P–S–HPC from Peanut Meal. The peanut meal (Henan, China) was purchased from Taobao (www.taobao.com). After freeze-drying, the peanut meal and the activation agent with a certain mass ratio (1:2) were fully ground in a mortar. The activation agent was a mixture of ZnCl_2 and $\text{Mg}(\text{NO}_3)_2 \cdot 6\text{H}_2\text{O}$ (mass ratio is

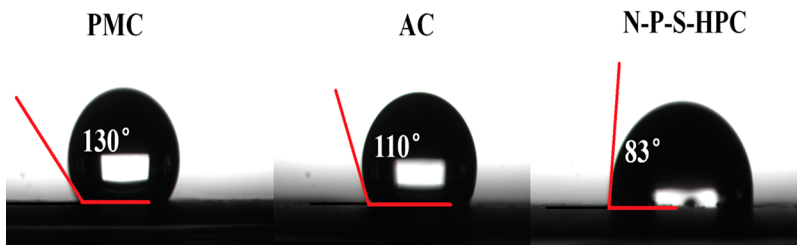


Figure 3. Water contact angles of PMC, AC, and N-P-S-HPC.

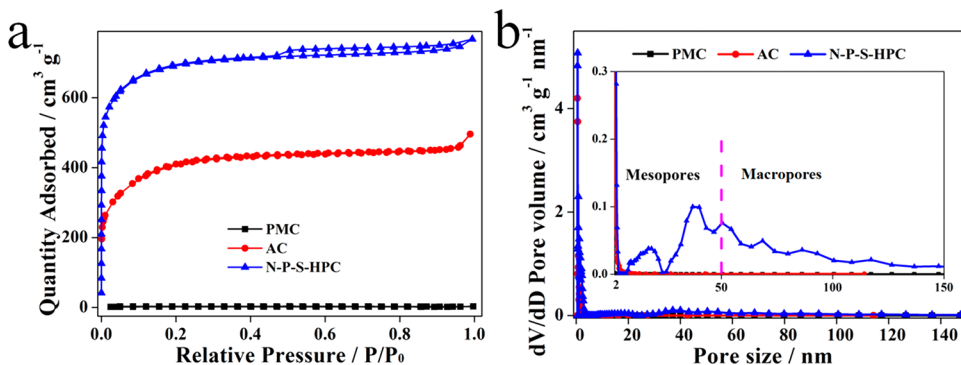


Figure 4. (a) N_2 adsorption–desorption isotherms and (b) pore size distributions of PMC, AC, and N-P-S-HPC.

1:1). The mixture was transferred into a crucible and then heated at 800 °C for 2 h (5 °C min⁻¹) under a N_2 flow. In order to remove the inorganic salt, the obtained sample was soaked in 6 M HCl at 60 °C for 12 h. Then the mixture was washed by deionized water to pH = 7 and dried at 100 °C (24 h). The obtained sample was named as N-P-S-HPC. For comparison, the peanut meal was carbonized at the same conditions in the absence of ZnCl_2 and $\text{Mg}(\text{NO}_3)_2 \cdot 6\text{H}_2\text{O}$, and the obtained sample was marked as PMC. In order to explore the effect of carbonation temperature, the mixture was also heated at 600 and 1000 °C under the same conditions and denoted as N-P-S-HPC-600 and N-P-S-HPC-1000, respectively. Furthermore, samples treated using different ratios of peanut meal to activation agent (1:1 and 1:4) and different activation agents (ZnCl_2 or $\text{Mg}(\text{NO}_3)_2 \cdot 6\text{H}_2\text{O}$ solely) were also prepared and marked as N-P-S-HPC-1, N-P-S-HPC-4, N-P-S-HPC-Zn, and N-P-S-HPC-Mg, respectively. The electrochemical performance of AC (Norit DLC Supra 50) was also investigated. For detailed characterizations and measurements, please refer to the Supporting Information.

RESULTS AND DISCUSSION

The composition and crystallinity of PMC, AC, and N-P-S-HPC were measured by X-ray diffraction (XRD) and Raman measurements. The XRD patterns of PMC, AC, and N-P-S-HPC are displayed in Figure 1a, where the observed broad peak and weak one at about 23° and 43° are attributed to the diffraction of the (002) and (100) planes of graphite,^{35,36} respectively. Additionally, Raman spectra were tested to further confirm the structure of as-prepared samples as shown in Figure 1b, where the observed two distinctive peaks at about 1355 and 1594 cm^{-1} are attributed to the D band (the disorder or defects in the graphite structure) and the G band (the graphitic order),³⁶ respectively. The intensity ratio of the disorder or defects in the graphite structure to the graphitic order (I_D/I_G) indicates the disordered or defected degree of the carbon materials.^{36,37} The I_D/I_G values of PMC, AC, and N-P-S-HPC were calculated to be 0.86, 0.98 and 1.05, respectively. Higher I_D/I_G ratios of N-P-S-HPC implies that there are more sites for ion accommodation, resulting in the enhanced electrochemical performance.⁴⁸

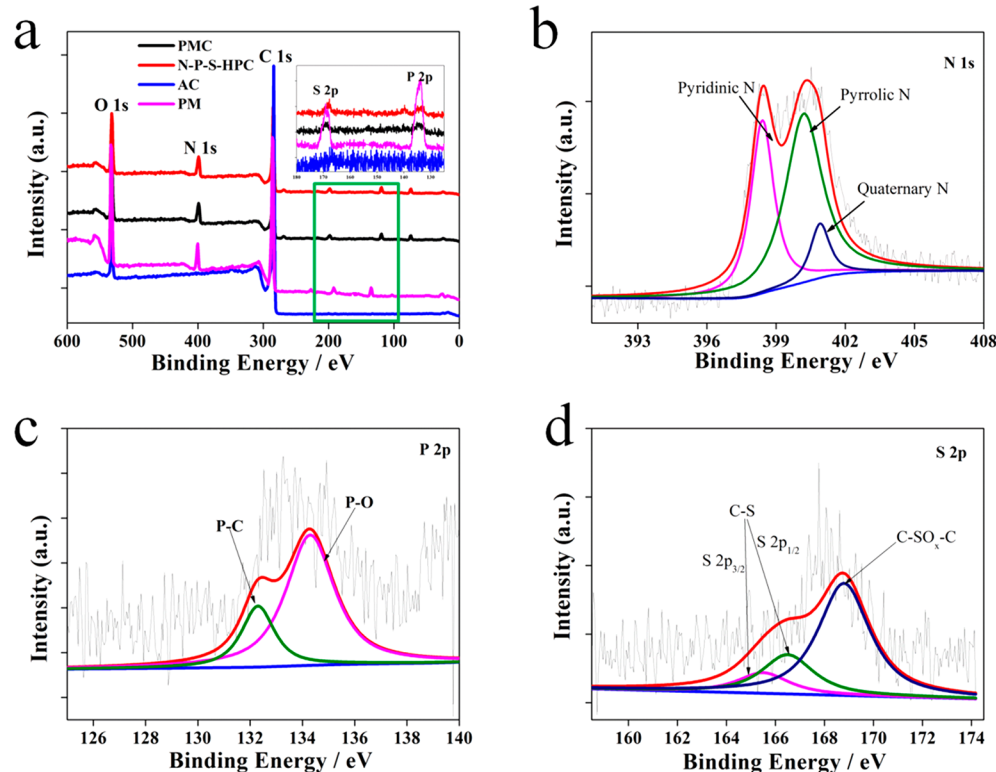
The surface microstructures and morphologies of PMC and N-P-S-HPC were characterized by scanning electron microscopy (SEM) and transmission electron microscopy (TEM) shown in Figure 2. It can be observed that PMC consists of blocklike structures with a relatively smooth surface (Figure 2a,b). After activation treatment, N-P-S-HPC displays a rough and fluffy 3D interconnected framework with silky carbon sheets (Figure 2c,d), which is helpful to the ion transport. To further explore the morphology of N-P-S-HPC, TEM (Figure 2e) and high-resolution transmission electron microscopy (HRTEM) (Figure 2f) measurements were conducted. It can be seen that the transparent carbon sheets are observed from the TEM image, which is consistent with the SEM image result. The porous structure of the N-P-S-HPC matrix is further demonstrated by HRTEM characterization.⁴⁹ Meanwhile, the selected area electron diffraction (SAED) pattern of N-P-S-HPC without a lattice structure is shown in the inset of Figure 2f, suggesting its amorphous feature. Elemental mappings of N-P-S-HPC in Figure 2g,h illustrate the uniform N, P, and S distribution. Water contact angles of PMC (130°), AC (110°), and N-P-S-HPC (83°) shown in Figure 3 illustrate that N-P-S-HPC shows the best wettability to the electrolyte, which is beneficial to the ion transfer.

To further investigate the porous structures of PMC, AC, and N-P-S-HPC, N_2 adsorption/desorption isotherms and pore size distributions are displayed in Figure 4. It is obvious in Figure 4a that PMC without activation discloses a nonporous surface, while N-P-S-HPC displays a Type I isotherm with a bit of a hysteresis loop at relative pressure (P/P_0) higher than 0.4, indicating the existence of plenty of micropores, mesopores, and macropores.⁵⁰ In the meantime, AC shows the Type I isotherm characteristic without an obvious hysteresis loop, suggesting the existence of rich micropores.^{41,51} The pore size distributions of PMC, AC, and N-P-S-HPC are calculated according to the density functional theory (DFT) method and shown in Figure 4b and Table 1. It

Table 1. Specific Surface Areas (S), Total Pore Volumes (V_{total}), and Elemental Contents of AC, PM, PMC, and N–P–S–HPC

	$S_{\text{BET}}^{\text{a}}$ ($\text{m}^2 \text{ g}^{-1}$)	$S_{\text{mic}}^{\text{b}}$ ($\text{m}^2 \text{ g}^{-1}$)	$S_{\text{ext}}^{\text{c}}$ ($\text{m}^2 \text{ g}^{-1}$)	V_{total} ($\text{cm}^3 \text{ g}^{-1}$)	content (atomic %)				
					C	O	N	P	S
AC	1484	1346	138	0.36	91	9			
PM					69.1	20.4	7	2.5	1
PMC	6.6	3.3	3.3	0.003	75	11.4	12.1	0.83	0.65
N–P–S–HPC	2090	1481	609	1.42	78.4	8.9	11.2	0.82	0.64

^aThe S are analyzed by the Brunauer–Emmett–Teller model. ^bThe S of micropores. ^cThe S of other pores.

**Figure 5.** XPS spectra (a) of PM, PMC, AC, and N–P–S–HPC. High-resolution XPS spectra of N 1s (b), P 2p (c), and S 2p (d) for N–P–S–HPC.

can be seen that PMC exhibits a less porous structure. Meanwhile, the pore size distribution curve of AC (Figure 4b) demonstrates that the pore network mainly consists of rich micropores. Compared to PMC and AC, N–P–S–HPC has a hierarchical pore structure mainly consisting of micropores, mesopores, and macropores, which is consistent with the N_2 adsorption/desorption isotherms. The S_{BET} and V_{total} of N–P–S–HPC ($2090 \text{ m}^2 \text{ g}^{-1}$ and $1.42 \text{ cm}^3 \text{ g}^{-1}$) are higher than those of PMC ($6.6 \text{ m}^2 \text{ g}^{-1}$, $0.003 \text{ cm}^3 \text{ g}^{-1}$) and AC ($1484 \text{ m}^2 \text{ g}^{-1}$, $0.36 \text{ cm}^3 \text{ g}^{-1}$), implying that N–P–S–HPC has a superior rate capability. Furthermore, in order to investigate the influence of activation agent, N_2 adsorption–desorption isotherms of N–P–S–HPC-Zn and N–P–S–HPC-Mg were also examined for comparison. From Figure S1 and Table S1, it can be seen that N–P–S–HPC possesses the largest specific surface area and total pore volumes, proving the synergistic effects of $ZnCl_2$ and $Mg(NO_3)_2$ on improving the specific surface area and total pore volume.

To further confirm the surface chemical composition and elemental bond states of PM, PMC, AC, and N–P–S–HPC, XPS measurement was carried out (Figure 5). As shown in Figure 5a, the full scan spectra depict the existence of C, O, N, P, and S in PM, PMC, and N–P–S–HPC, which is in accordance with the element mapping results. Meanwhile, the

survey spectrum of AC only shows C and O signals. The corresponding elemental contents are listed in Table 1. Obviously, the N, P, and S contents in both PMC and N–P–S–HPC are similar, indicating that activation treatment will not destroy the elemental composition of PMC, AC, and N–P–S–HPC. The N 1s, P 2p, and S 2p of N–P–S–HPC are shown in Figure 5b–d to reveal the doping degree of heteroatoms in the carbon matrix in detail. In Figure 5b, the N 1s spectrum can be fitted into three parts including pyridinic-N (N-6, 398.4 eV), pyridone/pyrrolic-N (N-5, 400.2 eV), and quaternary-N (N-Q, 401.3 eV).^{53,54} It is worth mentioning that N-6 and N-5 can contribute to pseudocapacitance to enhance the capacitance performance.^{53,54} In addition, N-Q can promote the electrical conductivity of the bulk carbon and facilitate the electron transfer ability.^{53,54} The P 2p spectrum is resolved into two peaks at 134.2 and 132.9 eV (Figure 5c), corresponding to P–O and C–P,⁵⁵ respectively. Meantime, the S 2p spectrum reveals the presence of three peaks, where one centered at 168.5 eV is attributed to C–SO_x–C bonding and the other two peaks at about 165.2 and 164.1 eV are assigned to S 2p_{1/2} and S 2p_{3/2} of C–S bonding,^{56,57} respectively, as shown in Figure 5d. The introduction of P and S can also donate active sites for improving the specific capacitance.^{2,9} The XPS analysis further

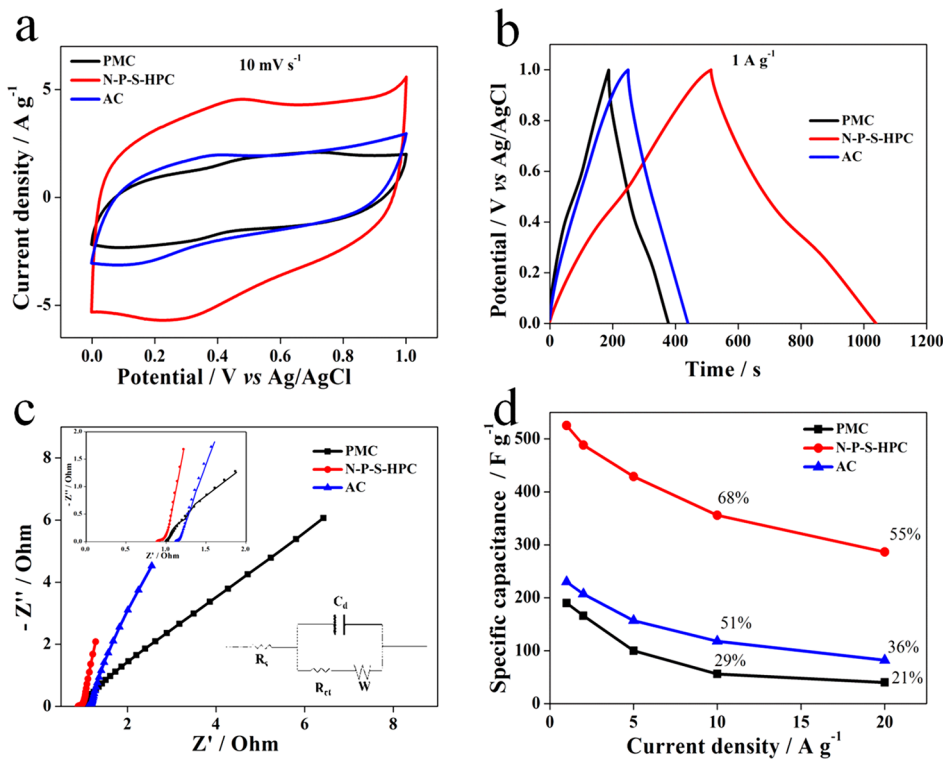


Figure 6. In a three-electrode system, electrochemical performances were tested in 1 M H₂SO₄. (a) CV curves (10 mV s⁻¹) of PMC, AC, and N–P–S–HPC, (b) GCD curves (1 A g⁻¹) of PMC, AC, and N–P–S–HPC. (c) Nyquist plots of PMC, AC, and N–P–S–HPC. Inset of part c is the fitted lines and equivalent electric circuit. (d) Specific capacitances of PMC, AC, and N–P–S–HPC from 1 to 20 A g⁻¹.

Table 2. Summary of Electrochemical Performances of Biomass Converted Carbon Materials

biomass precursor	S_{BET} (m ² g ⁻¹)	heteroatoms (atomic %)	C_m (F g ⁻¹) / (I/m) (A g ⁻¹) / electrolyte	E (Wh kg ⁻¹) / P(W kg ⁻¹) / electrolyte	ref
<i>Azadirachta indica</i>	1230		400/0.5/1 M H ₂ SO ₄		60
cow dung	2000		124/0.1/1 M Et ₄ NBF ₄ (2E)		61
tobacco rods	1994	N (1.3)	286.6/0.5/6 M KOH		52
human hair	1306		340/1/6 M KOH		62
shell of broad beans	655.4	N (2.0) S(0.9)	202/0.5/6 M KOH		63
corn straw	1771		222/1/6 M KOH		64
willow catkin	645	N (2.51)	340/0.1/6 M KOH		65
wheat flour	1294	N	383/1/1 M H ₂ SO ₄		36
willow catkin	1589	N (0.14)	298/0.5/6 M KOH	21/180/1 M Na ₂ SO ₄	34
pomelo mesocarps	974.6	N (9.12)	245/0.5/2 M KOH	14.7/90/1 M Na ₂ SO ₄	66
fungus (<i>Auricularia</i>)	1103		374/0.5/6 M KOH	22/100/1 M Na ₂ SO ₄	41
shrimp shells	1946	N (7.84)	322/0.5/6 M KOH	11.2/110/6 M KOH	67
yogurt	1300	N (12)	225/2/1 M H ₂ SO ₄	7/5000/6 M KOH	68
lignocellulose	1535	P	195/1/6 M KOH	4.7/100/6 M KOH	69
soybean	1749	N (2.55)	243.2/0.5/6 M KOH	12.5/450/0.5 M Na ₂ SO ₄	70
ant powder	2650	N (1.5) S (0.4)	352/0.1/6 M KOH	24/400/1 M Na ₂ SO ₄	71
gelatin	416	B (3.3) N (8.6)	268/0.1/1 M H ₂ SO ₄	8/6/1 M H ₂ SO ₄	40
vanillin	2347	N (2.24)	167.3/1/6 M KOH	10.8/45/6 M KOH	9
brussel sprouts	2410	N (1.13) S (0.03)	255/0.5/6 M KOH	6.4/50/6 M KOH	37
taro stems	1012	N (4.8)	263/0.1/6 M KOH	5.56/5/6 M KOH	38
peanut meal	2090	N (11.2), P (0.82) S (0.64)	525.3/1/1 M H ₂ SO ₄	24.9/400/1 M Na ₂ SO ₄	this work

confirms that N, P, and S have been incorporated into N–P–S–HPC carbon construction, leading to the improved capacitive performance by contributing the additional pseudocapacitance.^{54,56}

To estimate the electrochemical performances, electrochemical impedance spectroscopy (EIS), galvanostatic charge–discharge (GCD), and cyclic voltammetry (CV)

curves were tested in a three electrode system. The carbonization temperature and the ratio of activation agent are important parameters for the synthesis of N–P–S–HPC. The electrochemical behaviors of samples at different temperatures (600 °C, 800 °C, and 1000 °C) and different ratios (peanut meal–activation agents = 1:1, 1:2, 1:4) were measured (Figure S2). It can be seen that N–P–S–HPC (800 °C, peanut

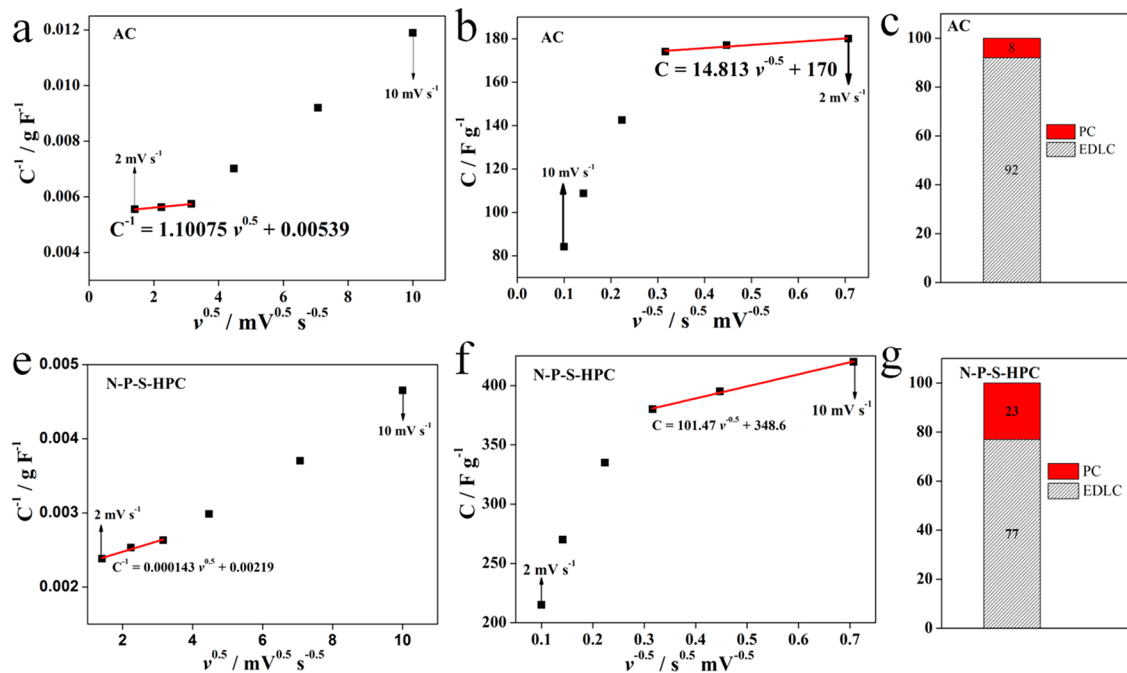


Figure 7. Capacitance contribution of AC (a–c) and N–P–S–HPC (d–f) were calculated by the Trasatti method (Supporting Information). Plot of C^{-1} vs $v^{0.5}$ for AC and N–P–S–HPC (a, d), Plot of C vs $v^{-0.5}$ for AC and N–P–S–HPC (b, e). Histogram for AC and N–P–S–HPC showing the capacitance contribution from EDLC and PC (c, f).

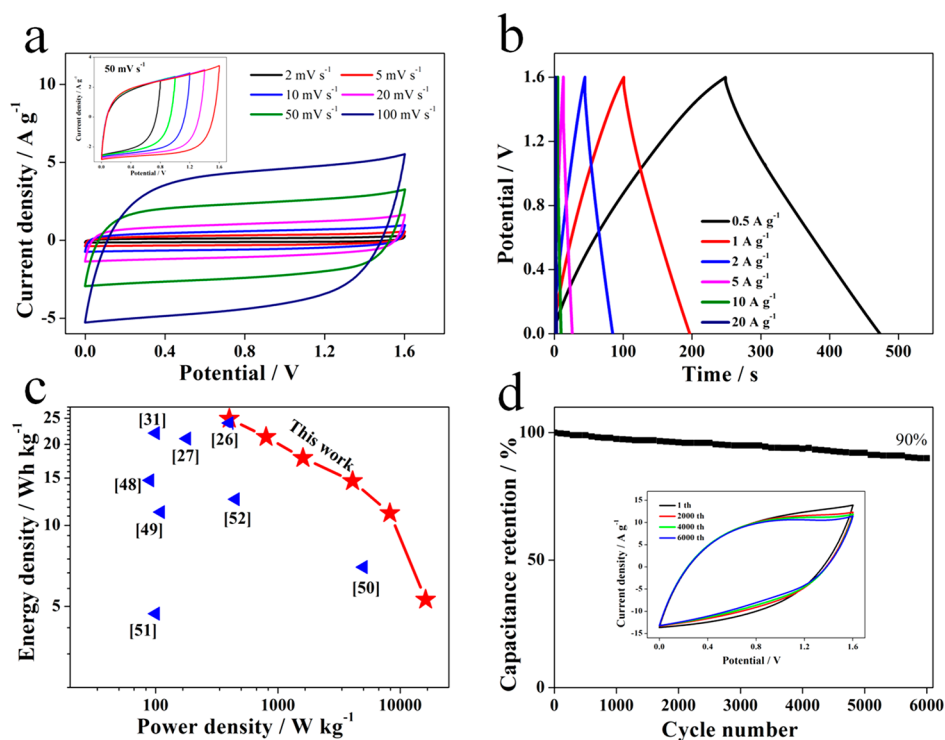


Figure 8. Electrochemical performance of N–P–S–HPC//N–P–S–HPC symmetric SCs: (a) CV curves (2–100 mV s⁻¹). Inset of part a is CV curves (50 mV s⁻¹). (b) GCD curves (0.5–20 A g⁻¹) at different current densities; (c) Ragone plots of N–P–S–HPC//N–P–S–HPC symmetric SCs; (d) capacitance retention of N–P–S–HPC//N–P–S–HPC symmetric SCs after the 6000th cycle (300 mV s⁻¹). Inset of part d is CV curves of 1st, 2000th, 4000th, and 6000th at 300 mV s⁻¹.

meal–activation agent = 1:2) displays the largest area of CV curves and longest discharge time of GCD curves than others, suggesting that N–P–S–HPC displays the better electrochemical performance. The electrochemical performances of PMC, AC, and N–P–S–HPC were shown in Figure 6. It is

obvious that CV curves of PMC and N–P–S–HPC present similar shapes and two weak redox peaks (0.25 V/0.4 V) caused by N within the potential range (0–1 V) at 1 A g⁻¹.¹⁷ The CV curve of N–P–S–HPC shows the larger area and a more rectangular shape than AC and PMC. The specific

capacitances of N–P–S-HPC, AC, and PMC are 525, 230, and 196 F g⁻¹ at 1 A g⁻¹ (Figure 6b) according to the GCD curves, respectively. The superior capacitive performance of N–P–S-HPC is higher than the other state-of-the-art values reported in the recent literature (Table 2), which is attributed to its large specific surface area (2090 m² g⁻¹), hierarchically porous framework structure, and N (11.2 atomic %), P (0.82 atomic %), and S (0.64 atomic %) codoping. To further investigate the dynamic behaviors of PMC, AC, and N–P–S-HPC, EIS measurement was conducted, as shown in Figure 6c, accompanied by a corresponding equivalent electric circuit and the fitted lines of Nyquist plots. The linear slope of N–P–S-HPC in the low frequency region is severely steep, indicating its faster ion diffusion in the electrolyte. In the high frequency region, N–P–S-HPC displays a lower $R_{ct} = 0.05 \Omega$ (charge transfer resistance) and $R_s = 0.9 \Omega$ (equivalent series resistance) than PMC ($R_{ct} = 0.11 \Omega$, $R_s = 1.10 \Omega$) and AC ($R_{ct} = 0.07 \Omega$, $R_s = 1.15 \Omega$), suggesting its fast charge transfer ability. From Figure 6d, N–P–S-HPC exhibits great capacitance retention (68% at 10 A g⁻¹, 55% at 20 A g⁻¹), much larger than those of AC (51% at 10 A g⁻¹, 36% at 20 A g⁻¹) and PMC (29% at 10 A g⁻¹, 21% at 20 A g⁻¹), implying its outstanding electrochemical performance at high current density.

In order to adequately understand the capacitive behavior of N–P–S-HPC, the capacitance differentiation of AC and N–P–S-HPC was calculated by Trasatti analysis as shown in Figure 7.^{58,59} The total capacitance (C_{Total} , Figure 7a,d) and the electrical double layer capacitance (C_{EDLC} , Figure 7b,e) can be estimated from the ordinate intercept according to Trasatti analysis, respectively. The pseudocapacitance (C_{PC}) can be estimated from the difference between C_{Total} and C_{EDLC} . The capacitance contributions of AC in $\leq 10 \text{ mV s}^{-1}$ (Figure 7a–c) from EDLC and PC values are 92% and 8% (Figure 7c), respectively. For N–P–S-HPC, it can be seen that the PC capacitance contribution reaches up to 23% as shown in Figure 7d–f, which is closely consistent with the Dunn method analysis results of N–P–S-HPC at 5 mV s⁻¹ (Figure S3), due to its N (11.2 atomic %), P (0.82 atomic %), and S (0.64 atomic %) codoping in the porous structure.

To further explore the practical application of N–P–S-HPC electrode, N–P–S-HPC//N–P–S-HPC symmetric SCs was assembled by two of the same N–P–S-HPC electrodes and measured in 1 M Na₂SO₄. The CV curves of the N–P–S-HPC//N–P–S-HPC symmetric SCs operated in different voltage windows at 50 mV s⁻¹ are shown in the inset of Figure 8a. It can be seen that the voltage window of N–P–S-HPC//N–P–S-HPC symmetric SCs ranges from 0 to 1.6 V. Figure 8a,b displays the CV curves of the N–P–S-HPC//N–P–S-HPC symmetric SCs (2–100 mV s⁻¹) and GCD curves (0.5–20 A g⁻¹), respectively. All of the CV curves and GCD curves show nearly rectangularlike shapes and triangular symmetry without obvious redox peaks, respectively, illustrating the characteristics of typical EDLC. Furthermore, the N–P–S-HPC//N–P–S-HPC symmetric SCs shows the satisfied energy density (24.9 Wh kg⁻¹ at 400 W kg⁻¹), which is obviously superior to previously reported biomass based carbon symmetric SCs in the aqueous electrolyte (Figure 8c and Table 2). The cycling stability of N–P–S-HPC//N–P–S-HPC symmetric SCs is shown in Figure 8d. It is noted that the capacitive retention reaches up to 90% after 6000 cycles at 300 mV s⁻¹. As a result, biomass converted N, P, S codoped porous carbon is suggested to be a potential candidate for SCs.

CONCLUSIONS

In summary, the N, P, and S self-doped hierarchically porous carbon derived from PM was successfully prepared via a facile one-step process by simultaneous carbonization and activation. The N–P–S-HPC doped by N (11.2 atomic %), P (0.82 atomic %), and S (0.64 atomic %) exhibits a hierarchical porous framework with a large surface area (2090 m² g⁻¹). The obtained N–P–S-HPC displays a rather large specific capacitance of 525 F g⁻¹ at 1 A g⁻¹, excellent rate performance (68% retention at 10 A g⁻¹), due to a typical hierarchically porous framework (micropores, mesopores, and macropores) with a large specific surface area, multiheteroatom (N, P, and S) codoping, improved hydrophilicity, and lower R_{ct} and R_s . Meanwhile, the N–P–S-HPC//N–P–S-HPC symmetric SCs display a maximum energy density (24.9 Wh kg⁻¹ at 400 W kg⁻¹) in 1 M Na₂SO₄. After the 6000th cyclic voltammetry at 300 mV s⁻¹, the capacitance retention of the N–P–S-HPC//N–P–S-HPC symmetric SCs reaches up to 90%, indicating excellent cycling stability. The heteroatoms codoped biomass based hierarchically porous carbon should be considerably promising for energy storage applications.

ASSOCIATED CONTENT

Supporting Information

The Supporting Information is available free of charge on the ACS Publications website at DOI: [10.1021/acssuschemeng.9b00725](https://doi.org/10.1021/acssuschemeng.9b00725).

Material characterization; N₂ adsorption–desorption isotherms of N–P–S-HPC-Zn, N–P–S-HPC-Mg, and N–P–S-HPC; electrochemical performances of all samples; Dunn method analysis of respective capacitance contribution of N–P–S-HPC; and S_{BET} and V_{total} of N–P–S-HPC-Zn, N–P–S-HPC-Mg, and N–P–S-HPC (PDF)

AUTHOR INFORMATION

Corresponding Authors

*Phone: +8621 62234322. E-mail: bhsjy64@163.com.

*E-mail: tlu@phy.ecnu.edu.cn.

ORCID

Ting Lu: [0000-0002-0492-4900](https://orcid.org/0000-0002-0492-4900)

Likun Pan: [0000-0001-9294-1972](https://orcid.org/0000-0001-9294-1972)

Notes

The authors declare no competing financial interest.

ACKNOWLEDGMENTS

The authors sincerely acknowledge financial support from Science and Technology Development Program Project of Jilin Province in 2017 (Grant 20170203001SF), Outstanding Youth Talents in Anhui Provincial Education Department (Grant 2017GXBJZD47), National Public Welfare Special Foundation (Grant 201504502), Important Project of Anhui Provincial Education Department (Grant KJ2018A0446), and The Scientific Research Foundation of Suzhou University (Grant 2018SZXYDZXZ02).

REFERENCES

- Chen, Y.; Cai, K.; Liu, C.; Song, H.; Yang, X. High-performance and Breathable Polypyrrole Coated Air-laid Paper for Flexible All-solid-state Supercapacitors. *Adv. Energy Mater.* **2017**, *7*, 1701247.

- (2) Yang, J.; Zhou, X.; Wu, D.; Zhao, X.; Zhou, Z. S-doped N-rich Carbon Nanosheets with Expanded Interlayer Distance as Anode Materials for Sodium-ion Batteries. *Adv. Mater.* **2017**, *29*, 1604108.
- (3) Le, V.; Do, T.; Retamal, J. R. D.; Shao, P.; Lai, Y.; Wu, W.; He, J.; Chueh, Y.; Chu, Y. Van der Waals Heteroepitaxial AZO/NiO/AZO/Muscovite (ANA/muscovite) Transparent Flexible Memristor. *Nano Energy* **2019**, *56*, 322–329.
- (4) Wang, Y.; Xia, Y. Recent Progress In Supercapacitors: from Materials Design to System Construction. *Adv. Mater.* **2013**, *25*, 5336–5342.
- (5) Zhang, S.; Pan, N. Supercapacitors Performance Evaluation. *Adv. Energy Mater.* **2015**, *5*, 1401401.
- (6) Das, S.; Hossain, M. J.; Leung, S. F.; Lenox, A.; Jung, Y.; Davis, K.; He, J.; Roy, T. A Leaf-inspired Photon Management Scheme Using Optically Tuned Bilayer Nanoparticles for Ultra-thin and Highly Efficient Photovoltaic Devices. *Nano Energy* **2019**, *58*, 47–56.
- (7) Ehrmaier, J.; Domcke, W.; Opalka, D. Mechanism of Photocatalytic Water Oxidation by Graphitic Carbon Nitride. *J. Phys. Chem. Lett.* **2018**, *9*, 4695–4699.
- (8) Han, S.; Pu, Y. C.; Zheng, L.; Hu, L.; Zhang, J.; Fang, X. Uniform Carbon-Coated CdS Core-shell Nanostructures: Synthesis, Ultrafast Charge Carriers Dynamics, and Photoelectrochemical Water Splitting. *J. Mater. Chem. A* **2016**, *4*, 1078–1086.
- (9) Liu, Y.; Cao, L.; Luo, J.; Peng, Y.; Ji, Q.; Dai, J.; Zhu, J.; Liu, X. Biobased Nitrogen- and Oxygen-Codoped Carbon Materials for High-Performance Supercapacitor. *ACS Sustainable Chem. Eng.* **2019**, *7*, 2763–2773.
- (10) Li, J.; Han, L.; Zhang, X.; Zhu, G.; Chen, T.; Lu, T.; Pan, L. Sb₂O₅/Co-containing Carbon Polyhedra as Anode Material for High-performance Lithium-ion Batteries. *Chem. Eng. J.* **2019**, *370*, 800–809.
- (11) Zhong, C.; Deng, Y.; Hu, W.; Qiao, J.; Zhang, L.; Zhang, J. A Review of Electrolyte Materials and Compositions for Electrochemical Supercapacitors. *Chem. Soc. Rev.* **2015**, *44*, 7484–7539.
- (12) Zhi, M.; Xiang, C.; Li, J.; Li, M.; Wu, N. Nanostructured Carbon-metal Oxide Composite Electrodes for Supercapacitors: A Review. *Nanoscale* **2013**, *5*, 72–88.
- (13) Strauss, V.; Marsh, K.; Kowal, M. D.; El-Kady, M.; Kaner, R. B. A Simple Route to Porous Graphene from Carbon Nanodots for Supercapacitor Applications. *Adv. Mater.* **2018**, *30*, 1704449.
- (14) Fan, P.; Ren, J.; Pang, K.; Cheng, Y.; Wu, X.; Zhang, Z.; Ren, J.; Huang, W.; Song, R. Cellulose-Solvent-Assisted, One-Step Pyrolysis to Fabricate Heteroatoms-Doped Porous Carbons for Electrode Materials of Supercapacitors. *ACS Sustainable Chem. Eng.* **2018**, *6*, 7715–7724.
- (15) Zhang, L. L.; Zhao, X. S. Carbon-based Materials as Supercapacitor Electrodes. *Chem. Soc. Rev.* **2009**, *38*, 2520–2531.
- (16) Borenstein, A.; Hanna, O.; Attias, R.; Luski, S.; Brousse, T.; Aurbach, D. Carbon-based Composite Materials for Supercapacitor Electrodes: A Review. *J. Mater. Chem. A* **2017**, *5*, 12653–12672.
- (17) Chen, L. F.; Lu, Y.; Yu, L.; Lou, X. W. Designed Formation of Hollow Particle-based Nitrogen-doped Carbon Nanofibers for High-performance Supercapacitors. *Energy Environ. Sci.* **2017**, *10*, 1777–1783.
- (18) Kumar, R.; Joanni, E.; Singh, R. K.; Singh, D. P.; Moshkalev, S. A. Recent Advances in The Synthesis and Modification of Carbon-based 2D Materials for Application in Energy Conversion and Storage. *Prog. Energy Combust. Sci.* **2018**, *67*, 115–157.
- (19) Wang, Y.; Shi, Z.; Huang, Y.; Ma, Y.; Wang, C.; Chen, M.; Chen, Y. Supercapacitor Devices Based on Graphene Materials. *J. Phys. Chem. C* **2009**, *113*, 13103–13107.
- (20) Futaba, D. N.; Hata, K.; Yamada, T.; Hiraoka, T.; Hayamizu, Y.; Kakudate, Y.; Tanaike, O.; Hatori, H.; Yumura, M.; Iijima, S. Shape-engineerable and Highly Densely Packed Single-walled Carbon Nanotubes and Their Application as Super-capacitor Electrodes. *Nat. Mater.* **2006**, *5*, 987–994.
- (21) Long, C.; Zhuang, J.; Xiao, Y.; Zheng, M.; Hu, H.; Dong, H.; Lei, B.; Zhang, H.; Liu, Y. Nitrogen-doped Porous Carbon with an Ultrahigh Specific Surface Area for Superior Performance Supercapacitors. *J. Power Sources* **2016**, *310*, 145–153.
- (22) Cai, J.; Niu, H.; Li, Z.; Du, Y.; Cizek, P.; Xie, Z.; Xiong, H.; Lin, T. High-Performance Supercapacitor Electrode Materials from Cellulose-Derived Carbon Nanofibers. *ACS Appl. Mater. Interfaces* **2015**, *7* (27), 14946–14953.
- (23) Huang, Z. H.; Liu, T. Y.; Song, Y.; Li, Y.; Liu, X. X. Balancing the Electrical Double Layer Capacitance and Pseudocapacitance of Heteroatom Doped Carbon. *Nanoscale* **2017**, *9*, 13119–13127.
- (24) Chen, L.; Chen, Z.; Kuang, Y.; Xu, C.; Yang, L.; Zhou, M.; He, B.; Jing, M.; Li, Z.; Li, F.; Chen, Z.; Hou, Z. Edge-rich Quasi-mesoporous Nitrogen-doped Carbon Framework Derived from Palm Tree Bark Hair for Electrochemical Applications. *ACS Appl. Mater. Interfaces* **2018**, *10*, 27047–27055.
- (25) Long, C.; Qi, D.; Wei, T.; Yan, J.; Jiang, L.; Fan, Z. Nitrogen-doped Carbon Networks for High Energy Density Supercapacitors Derived from Polyaniline Coated Bacterial Cellulose. *Adv. Funct. Mater.* **2014**, *24*, 3953–3961.
- (26) Shu, Y.; Maruyama, J.; Iwasaki, S.; Maruyama, S.; Shen, Y.; Uyama, H. Nitrogen-doped Biomass/Polymer Composite Porous Carbons for High Performance Supercapacitor. *J. Power Sources* **2017**, *364*, 374–382.
- (27) Niu, J.; Shao, R.; Liang, J.; Dou, M.; Li, Z.; Huang, Y.; Wang, F. Biomass-derived Mesopore-dominant Porous Carbons with Large Specific Surface Area and High Defect Density as High Performance Electrode Materials for Li-ion Batteries and Supercapacitors. *Nano Energy* **2017**, *36*, 322–330.
- (28) Li, Y.; Liu, Y.; Wang, M.; Xu, X.; Lu, T.; Sun, C. Q.; Pan, L. Phosphorus-doped 3D Carbon Nanofiber Aerogels Derived from Bacterial-cellulose for Highly-efficient Capacitive Deionization. *Carbon* **2018**, *130*, 377–383.
- (29) Zhang, J.; Fang, J.; Han, J.; Yan, T.; Shi, L.; Zhang, D. N, P, S Co-doped Hollow Carbon Polyhedra Derived from MOF-based Core-shell Nanocomposites for Capacitive Deionization. *J. Mater. Chem. A* **2018**, *6*, 15245–15252.
- (30) Yan, L.; Li, D.; Yan, T.; Chen, G.; Shi, L.; An, Z.; Zhang, D. N,P,S-Co-doped Hierarchically Porous Carbon Spheres with Well-Balanced Gravimetric/Volumetric Capacitance for Supercapacitors. *ACS Sustainable Chem. Eng.* **2018**, *6* (4), 5265–5272.
- (31) Ling, Z.; Wang, Z.; Zhang, M.; Yu, C.; Wang, G.; Dong, Y.; Liu, S.; Wang, Y.; Qiu, J. S. Sustainable Synthesis and Assembly of Biomass-derived B/N Co-doped Carbon Nanosheets with Ultrahigh Aspect Ratio for High-performance Supercapacitors. *Adv. Funct. Mater.* **2016**, *26*, 111–119.
- (32) Li, Y.; Zhu, G.; Huang, H.; Xu, M.; Lu, T.; Pan, L. A N, S Dual Doping Strategy via Electrospinning to Prepare Hierarchically Porous Carbon Polyhedra Embedded Carbon Nanofibers for Flexible Supercapacitors. *J. Mater. Chem. A* **2019**, *7*, 9040–9050.
- (33) Zou, B. X.; Gao, Y.; Liu, B.; Yu, Y.; Lu, Y. Three Dimensional Heteroatom-doped Carbon Composite Film for Flexible Solid-state Supercapacitors. *RSC Adv.* **2016**, *6*, 4483–4489.
- (34) Li, Y.; Wang, G.; Wei, T.; Fan, Z.; Yan, P. Nitrogen and Sulfur Co-doped Porous Carbon Nanosheets Derived from Willow Catkin for Supercapacitors. *Nano Energy* **2016**, *19*, 165–175.
- (35) Wang, X.; Yun, S.; Fang, W.; Zhang, C.; Liang, X.; Lei, Z.; Liu, Z. Layer-Stacking Activated Carbon Derived from Sunflower Stalk as Electrode Materials for High-Performance Supercapacitors. *ACS Sustainable Chem. Eng.* **2018**, *6*, 11397–11407.
- (36) Yu, P.; Zhang, Z.; Zheng, L.; Teng, F.; Hu, L.; Fang, X. A Novel Sustainable Flour Derived Hierarchical Nitrogen-Doped Porous Carbon/Polyaniline Electrode for Advanced Asymmetric Supercapacitors. *Adv. Energy Mater.* **2016**, *6*, 1601111.
- (37) Li, J.; Zan, G.; Wu, Q. Nitrogen and Sulfur Self-doped Porous Carbon from Brussels Sprouts as Electrode Materials for High Stable Supercapacitors. *RSC Adv.* **2016**, *6*, 57464–57472.
- (38) He, D.; Zhao, W.; Li, P.; Liu, Z.; Wu, H.; Liu, L.; Han, K.; Liu, L.; Wan, Q.; Butt, F. K.; Qu, X. Bifunctional Biomass-derived 3D Nitrogen-doped Porous Carbon for Oxygen Reduction Reaction and Solid-state Supercapacitor. *Appl. Surf. Sci.* **2019**, *465*, 303–312.

- (39) Li, Y.; Zheng, K.; Ali Shah, S. A.; Huang, Y.; Tian, Y.; Cheng, J.; Zhang, J. Winter-Jujube-derived Carbon with Self-doped Heteroatoms and A Hierarchically Porous Structure for High-performance Supercapacitors. *RSC Adv.* 2017, 7, 43356–43365.
- (40) He, X.; Ling, P.; Qiu, J. S.; Yu, M.; Zhang, X.; Yu, C.; Zheng, M. Efficient Preparation of Biomass-based Mesoporous Carbons for Supercapacitors with both High Energy Density and High Power Density. *J. Power Sources* 2013, 240, 109–113.
- (41) Long, C.; Chen, X.; Jiang, L.; Zhi, L.; Fan, Z. Porous Layer-stacking Carbon Derived from In-built Template in Biomass for High Volumetric Performance Supercapacitors. *Nano Energy* 2015, 12, 141–151.
- (42) Lu, Y.; Zhang, S.; Yin, J.; Bai, C.; Zhang, J.; Li, Y.; Yang, Y.; Ge, Z.; Zhang, M.; Wei, L.; Ma, M.; Ma, Y.; Chen, Y. Mesoporous Activated Carbon Materials with Ultrahigh Mesopore Volume and Effective Specific Surface Area for High Performance Supercapacitors. *Carbon* 2017, 124, 64–71.
- (43) Gao, N.; Fang, X. Synthesis and Development of Graphene-inorganic Semiconductor Nanocomposites. *Chem. Rev.* 2015, 115, 8294–8343.
- (44) Duran Retamal, J. R.; Ho, C.-H.; Tsai, K.-T.; Ke, J.-j.; He, J.-H. Self-organized Al Nanotip Electrodes for Achieving Ultralow-Power and Error-Free Memory. *IEEE Trans. Electr. Dev.* 2019, 66, 938–943.
- (45) Zheng, L.; Han, S.; Liu, H.; Yu, P.; Fang, X. Hierarchical MoS₂ Nanosheet@TiO₂ Nanotube Array Composites with Enhanced Photocatalytic and Photocurrent Performances. *Small* 2016, 12 (11), 1527–1536.
- (46) Wang, Q.; Yan, J.; Wang, Y. B.; Wei, T.; Zhang, M. L.; Jing, X.; Fan, Z. Three-dimensional Flower-like and Hierarchical Porous Carbon Materials as High-rate Performance Electrodes for Supercapacitors. *Carbon* 2014, 67, 119–127.
- (47) Zhao, C.; Huang, Y.; Zhao, C.; Shao, X.; Zhu, Z. Rose-derived 3D Carbon Nanosheets for High Cyclability and Extended Voltage Supercapacitors. *Electrochim. Acta* 2018, 291, 287–296.
- (48) Pei, Z.; Li, H.; Huang, Y.; Xue, Q.; Huang, Y.; Zhu, M.; Wang, Z.; Zhi, C. Texturing in-situ: N, S-enriched Hierarchically Porous Carbon as Highly Active Reversible Oxygen Electrocatalyst. *Energy Environ. Sci.* 2017, 10, 742–749.
- (49) Yang, J.; Sun, H.; Liang, H.; Ji, H.; Song, L.; Gao, C.; Xu, H. A Highly Efficient Metal-free Oxygen Reduction Electrocatalyst Assembled from Carbon Nanotubes and Graphene. *Adv. Mater.* 2016, 28, 4606–4613.
- (50) Feng, Y.; Yao, J. Design of Melamine Sponge-Based Three-Dimensional Porous Materials toward Applications. *Ind. Eng. Chem. Res.* 2018, 57, 7322–7330.
- (51) Niu, J.; Liang, J.; Shao, R.; Liu, M.; Dou, M.; Li, Z.; Huang, Y.; Wang, F. Tremella-like N,O-co-doped Hierarchically Porous Carbon Nanosheets as High-performance Anode Materials for High Energy and Ultrafast Na-ion capacitors. *Nano Energy* 2017, 41, 285–292.
- (52) Zhao, Y.-Q.; Lu, M.; Tao, P.-Y.; Zhang, Y.-J.; Gong, X.-T.; Yang, Z.; Zhang, G.-Q.; Li, H.-L. Hierarchically Porous and Heteroatom Doped Carbon Derived from Tobacco Rods for Supercapacitors. *J. Power Sources* 2016, 307, 391–400.
- (53) Deng, Y.; Xie, Y.; Zou, K.; Ji, X. Review on Recent Advances in Nitrogen-doped Carbons: Preparations and Applications in Supercapacitors. *J. Mater. Chem. A* 2016, 4, 1144–1173.
- (54) Zhu, C.; Wang, M.; Yang, G.; Lu, T.; Pan, L. N, P Dual-doped Hollow Carbon Spheres for High-performance Supercapacitors. *J. Solid State Electrochem.* 2017, 21, 3631–3640.
- (55) Chen, J.; Wei, H.; Chen, H.; Yao, W.; Lin, H.; Han, S. N/P Co-doped Hierarchical Porous Carbon Materials for Superior Performance Supercapacitors. *Electrochim. Acta* 2018, 271, 49–57.
- (56) Yu, X.; Kang, Y.; Park, H. S. Sulfur and Phosphorus Co-doping of Hierarchically Porous Graphene Aerogels for Enhancing Supercapacitor Performance. *Carbon* 2016, 101, 49–56.
- (57) Huo, S.; Liu, M.; Wu, L.; Liu, M.; Xu, M.; Ni, W.; Yan, Y.-M. Methanesulfonic Acid-assisted Synthesis of N/S Co-doped Hierarchically Porous Carbon for High Performance Supercapacitors. *J. Power Sources* 2018, 387, 81–90.
- (58) Lee, Y. H.; Chang, K. H.; Hu, C. C. Differentiate the Pseudocapacitance and Double-layer Capacitance Contributions for Nitrogen-doped Reduced Graphene Oxide in Acidic and Alkaline Electrolytes. *J. Power Sources* 2013, 227, 300–308.
- (59) Wang, J.; Polleux, J.; Lim, J.; Dunn, B. Pseudocapacitive Contributions to Electrochemical Energy Storage in TiO₂ (Anatase) Nanoparticles. *J. Phys. Chem. C* 2007, 111 (40), 14925–14931.
- (60) Biswal, M.; Banerjee, A.; Deo, M.; Ogale, S. From Dead Leaves to High Energy Density Supercapacitors. *Energy Environ. Sci.* 2013, 6, 1249–1259.
- (61) Bhattacharjya, D.; Yu, J. S. Activated Carbon Made from Cow Dung as Electrode Material for Electrochemical Double Layer Capacitor. *J. Power Sources* 2014, 262, 224–231.
- (62) Qian, W.; Sun, F.; Xu, Y.; Qiu, L.; Liu, C.; Wang, S.; Yan, F. Human Hair-derived Carbon Flakes for Electrochemical Supercapacitors. *Energy Environ. Sci.* 2014, 7, 379–386.
- (63) Xu, G.; Han, J.; Ding, B.; Nie, P.; Pan, J.; Dou, H.; Li, H.; Zhang, X. Biomass-derived Porous Carbon Materials with Sulfur and Nitrogen Dual-doping for Energy Storage. *Green Chem.* 2015, 17, 1668–1674.
- (64) Lu, Y.; Zhang, S.; Yin, J.; Bai, C.; Zhang, J.; Li, Y.; Yang, Y.; Ge, Z.; Zhang, M.; Wei, L.; Ma, M.; Ma, Y.; Chen, Y. Mesoporous Activated Carbon Materials with Ultrahigh Mesopore Volume and Effective Specific Surface Area for High Performance Supercapacitors. *Carbon* 2017, 124, 64–71.
- (65) Wang, K.; Zhao, N.; Lei, S.; Yan, R.; Tian, X.; Wang, J.; Song, Y.; Xu, D.; Guo, Q.; Liu, L. Promising Biomass-based Activated Carbons Derived from Willow Catkins for High Performance Supercapacitors. *Electrochim. Acta* 2015, 166, 1–11.
- (66) Peng, H.; Ma, G.; Sun, K.; Zhang, Z.; Yang, Q.; Lei, Z. Nitrogen-doped Interconnected Carbon Nanosheets from Pomelo Mesocarps for High Performance Supercapacitors. *Electrochim. Acta* 2016, 190, 862–871.
- (67) Tian, W.; Gao, Q.; Zhang, L.; Yang, C.; Li, Z.; Tan, Y.; Qian, W.; Zhang, H. Renewable Graphene-like Nitrogen-doped Carbon Nanosheets as Supercapacitor Electrodes with Integrated High Energy-power Properties. *J. Mater. Chem. A* 2016, 4, 8690–8699.
- (68) Wahid, M.; Parte, G.; Phase, D.; Ogale, S. Yogurt: A Novel Precursor for Heavily Nitrogen Doped Supercapacitor Carbon. *J. Mater. Chem. A* 2015, 3, 1208–1215.
- (69) Yi, J.; Qing, Y.; Wu, C.; Zeng, Y.; Wu, Y.; Lu, X.; Tong, Y. Lignocellulose-derived Porous Phosphorus-doped Carbon as Advanced Electrode for Supercapacitors. *J. Power Sources* 2017, 351, 130–137.
- (70) Lin, G.; Ma, R.; Zhou, Y.; Liu, Q.; Dong, X.; Wang, J. KOH Activation of Biomass-derived Nitrogen-doped Carbons for Supercapacitor and Electrocatalytic Oxygen Reduction. *Electrochim. Acta* 2018, 261, 49–57.
- (71) Zhao, G.; Chen, C.; Yu, D.; Sun, L.; Yang, C.; Zhang, H.; Sun, Y.; Besenbacher, F.; Yu, M. One-step Production of O-N-S Co-doped Three-dimensional Hierarchical Porous Carbons for High-performance Supercapacitors. *Nano Energy* 2018, 47, 547–555.